Universiteit van Amsterdam

Paleo island configurations in the Aegean Sea between 21 ka and the present

A thesis submitted in partial fulfillment for the
Bachelor of Science for Bèta-Gamma majoring in Earth Sciences

At the
Faculty of Science (FNWI)
and
Institute of Biodiversity and Ecosystem Dynamics (IBED)

By E.F.M. (Erik) Koene
erik.koene@student.uva.nl
6286631

Supervised by K.F. Rijsdijk (IBED)

July 2013

Contents

List of Figures

List of Tables

Abstract

The theory of island biogeography quantitatively links an island its biodiversity to its size and isolation from continental landmasses. On a timescale of tens of thousands of years this island configuration (i.e. size and isolation) is not static but changes along with relative sea level (RSL) variations relative to the landmass. Recent statistical biogeographic research used global mean sea level variations to assess the influence of changing island configurations on biodiversity. Changes in RSL are not uniform when ice caps melt, as the redistribution of mass also affects the Earth its gravity field, thus the sea surface level, and causes the solid Earth to deform under the new surface load distribution, displacing land relative to sea levels. These mechanisms are described with the generalized sea level equation (GSLE).

This research adapts the model SELEN 2.9 to solve the GSLE from 21 ka to the present in steps of 1 ky, using the ICE-5G ice cap reconstruction. The modeled RSL changes are used to construct maps of paleo island configurations in the Aegean Sea. Time-varying island configurations are assessed for 10 islands.

The results show that the islands in the Aegean Sea used to be larger and less isolated. Corfu and Lemnos used to be connected to the continent. Andros, Astypalaia, Gavdos and Skyros used to be over twice their current size. The theory of island biogeography predicts that all islands used to be able to carry more biodiverse species, thus it is predicted that these island experienced biogeographic repercussions as the RSL rose.

It is noted that the digital elevation model misrepresents shorelines causing up to 50% overestimations in area calculations. Tectonic movements were neglected which may have caused up to ± 20 meters vertical displacements for individual islands.

Chapter 1

Introduction

1.1 Island biogeography

Island size and isolation from other islands and continents are assumed to be the main controlling factors that determine the number and kind of island species. This theory of island ecology as a function of the spatial configuration of the islands (i.e. their size and isolation) was first proposed by MacArthur and Wilson (1963) as the *theory of island biogeography*. In short, small islands only have the capacity to carry small populations, leading to small gene pools. Isolated islands receive little new genetic input. The resulting little gene pool variations reduce the ability of species to evolve under changing conditions such as new emerging competing species or resource depletion (Paulay, 1994).

It was later noted that island size and isolation are not static through time due to changes in the *relative sea level* (RSL), the observed sea level change relative to a local landmass (Milne et al., 1999; Whittaker and Fernández-Palacios, 2006). A RSL fall of over 100 meters, the reasons for which will follow, likely causes islands to grow in size and could *connect* islands and continents that are currently separate. Island endemic species (uniquely present, usually through local niche evolution) compete poorly with continental species that encountered stronger competition during their evolution (Paulay, 1994). This means that prolonged connected islands and continents likely carry more continental species, even when separated by water today. Change in the RSL may thus be a controlling factor on the biodiversity of islands.

Two important mechanisms in RSL change are identified that significantly influence island ecology (Whittaker and Fernández-Palacios, 2006). First the volcanic island emergence and submergence life-cycle which plays on a time scale of millions of years (Whittaker et al., 2008). Island size however also fluctuates on a smaller time scale of tens of thousands of years along with climatically induced changes in the RSL (Whittaker and Fernández-Palacios, 2006). The main reason for climatically induced sea level change is the exchange of water in oceanic basins and (frozen) water in ice caps on land – growing ice caps cause sea levels to drop already by the volume change of fluid water, and vice versa (Douglas et al., 2001).

An example of the effects of RSL change on biodiversity can be found in the period since the last glacial maximum (21.000 years ago, abbreviated to 21 ka). Measurements of RSL show global sea levels were down to -130 meters (Lambeck and Chappell, 2001). The RSL around Britain at that point was about 100 meters lower than currently. This effectively connected Britain and its islands to the European continent, which left a legacy in the biotic composition of those islands: longer connected islands carry the most continental species (Williamson, 1981, as cited in Whittaker and Fernández-Palacios, 2006). The implication is that to correctly model island biodiversity for the past 21 ka, an island its configuration with variations in RSL on a scale of tens of thousands of years must be incorporated. Such research has recently been done using the global mean RSL change (Norder, 2012).

1.2 Sea level equation

Oceanographers have since long noted that regionally RSL can deviate from the mean RSL of the Earth. This can be seen for the Aegean Sea (Greece, Southeast Europe) in figure 1.1 from Pluet and Pirazzoli (1991): different positions in the Aegean sea show different RSL trends. These differences can be on the order of 10 m, such as between Chalkida (A' on figure 1.1) and Spetses (C and D on figure 1.1). The implication is that to correctly model island biodiversity through time in the Aegean Sea, one must not only use the mean RSL changes but use RSL variations in both time *and* space.

RSL change through time and space can be described with the *sea level equation*: an expression for worldwide sea level change in discrete time steps. The concepts behind this theory are described below, following Mitrovica and Milne (2003) and Spada et al. (2012).

The Earth its solid surface elevation is usually defined as the radial distance between the solid Earth and a reference sea level. The elevation below sea level, *bathymetry*, can be gauged directly. The elevation above the sea level, *topography*, can only be measured in reference to an *assumed* sea surface at that position. Often used for this assumed sea surface is the *geoid*: an imaginary surface around the Earth that connects all points of equal gravitational potential energy as that on the surface of the oceans. Its shape is governed by the distribution of mass within and on the surface of the Earth. The geoid can be used to provide a *datum*: an elevation that is defined to be of 0 height. The Earth its solid surface elevation can therefore be expressed as the distance between the solid Earth and the geoid.

One can quantify this topography T at spherical position ω and time t_j, by finding the distance between the solid Earth R and the geoid G using:

$$T(\omega, t_j) = R(\omega, t_j) - G(\omega, t_j). \tag{1.1}$$

A positive T thus denotes the height of the solid Earth above sea level, while a negative T denotes the depth of water between the ocean surface and the solid Earth. This can most readily be seen in figure 1.2. A property that derives from this definition is the easy distinction between land ($T \geq 0$) and sea ($T < 0$).

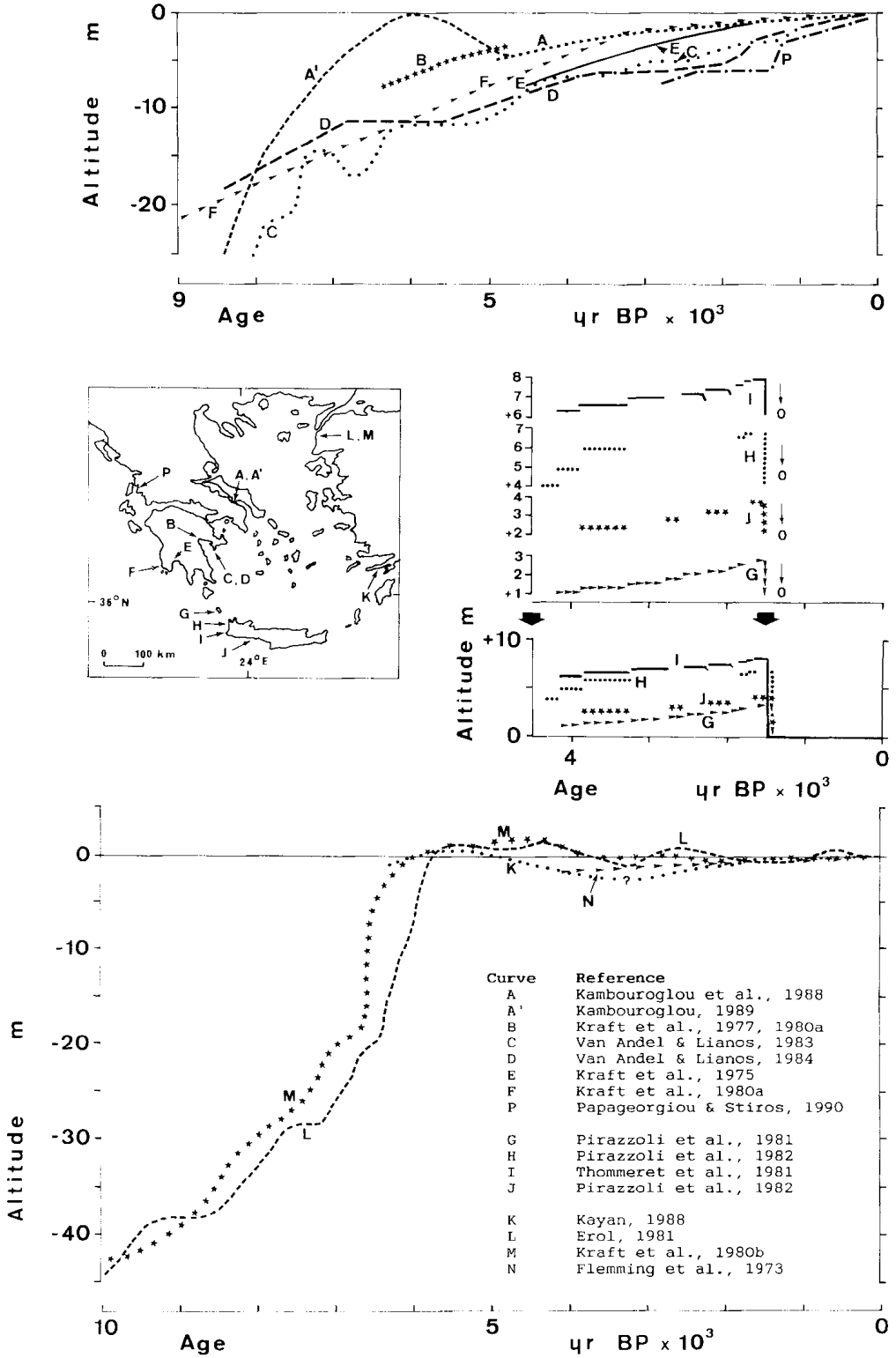

Figure 1.1: Holocene relative sea level curves in the Aegean Sea. The data has been sorted into 3 different regions and trends by their locations: A-F on the Greek mainland, G-J connected to Crete, K-M on the border with Turkey. The horizontal scale is the same in all figures, though data ranges differ. (Pluet and Pirazzoli, 1991).

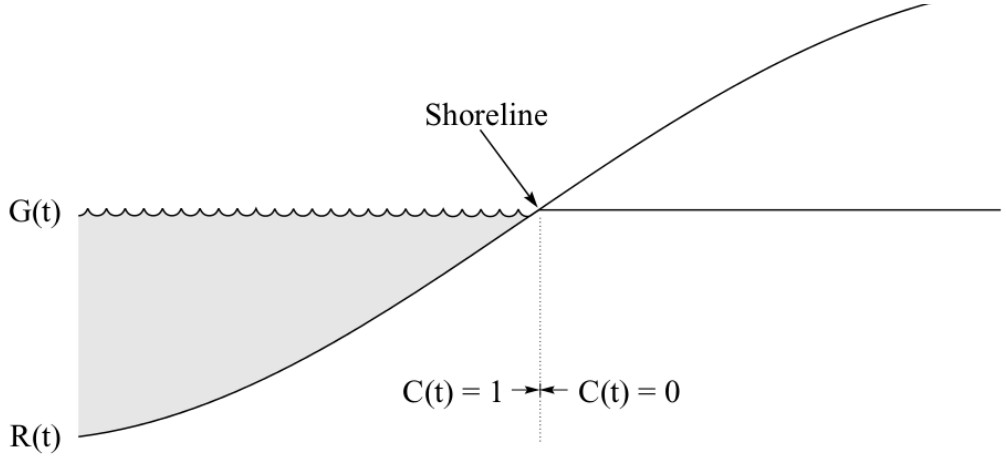

Figure 1.2: Graphical explanation of (1.1). G stands for the shape of the geoid, R denotes the Earth its solid surface. C denotes negative or positive $R - G$. The difference between G and R gives the bathymetry when the solid earth is smaller than the geoid, and gives the surface topography when the solid earth is larger than the geoid (e.g. in Dutch one says '10 meters above NAP', a chosen sea level in Amsterdam, which is similar to the difference between solid Earth level and assumed equipotential sea level, the geoid). (Mitrovica and Milne, 2003).

The theory of the sea level equation identifies three mechanisms that change the level of the geoid and solid Earth surface in space and time. See figure 1.3 for a graphical explanation of these mechanisms.

1. The first mechanism is the uniform geoid shift that occurs because of a change in grounded ice volume. As the volume of water locked in ice caps on land decreases, an opposite volume change of oceanic water is assumed. This increased ocean volume is accounted for by a global, uniform sea level rise, thus also a uniform geoid shift.

2. The second mechanism is the geoid perturbation because of a change in grounded ice mass. When a mass of ice accumulates on land, it creates a locally greater gravitational potential, thus a locally elevated geoid and sea level around the ice caps. This differently shaped geoid causes regional deviations up to $\pm 14\%$ on global sea level rises or falls (Woodward, 1888).

3. The third mechanism is the solid Earth deformation that occurs because of the redistribution of surface mass. Any mass on the Earth its surface stresses the ground beneath it. While the Earth its lithosphere, the topmost rheologically distinct layer of the Earth, is rigid and does not deform easily, the asthenosphere below it may deform under the applied stress. The response can be successfully modeled by approaching the Earth as a stratified viscoelastic Maxwell medium (Peltier, 1974). This means that both the deformation and relaxation – after applying and respectively removing the load – is made up of an instantaneous and an exponentially decreasing delayed response. Thus when ice caps or water masses grow, the solid Earth beneath it will subside immediately and keep subsiding until the delayed response dies out.

The astenospheric material under the loading will be displaced to the surrounding regions, causing an uplift of land around the loaded area. The speed and amount of deformation depend on the viscoelastic properties of the Earth model.

Lastly, a modelling step was identified and formalized by Mitrovica and Milne (2003) under the concept of *moving shorelines* to complete the *generalized sea level equation* (GSLE):

4. The mechanisms above can only be solved for assuming a constant ocean area. However, more land might get exposed as sea levels drop and thus shorelines migrate seawards: the ocean area actually changes along with RSL change. The volume of water that is calculated to end up below the solid Earth level must therefore be redistributed to fit in the shrunken ocean area.

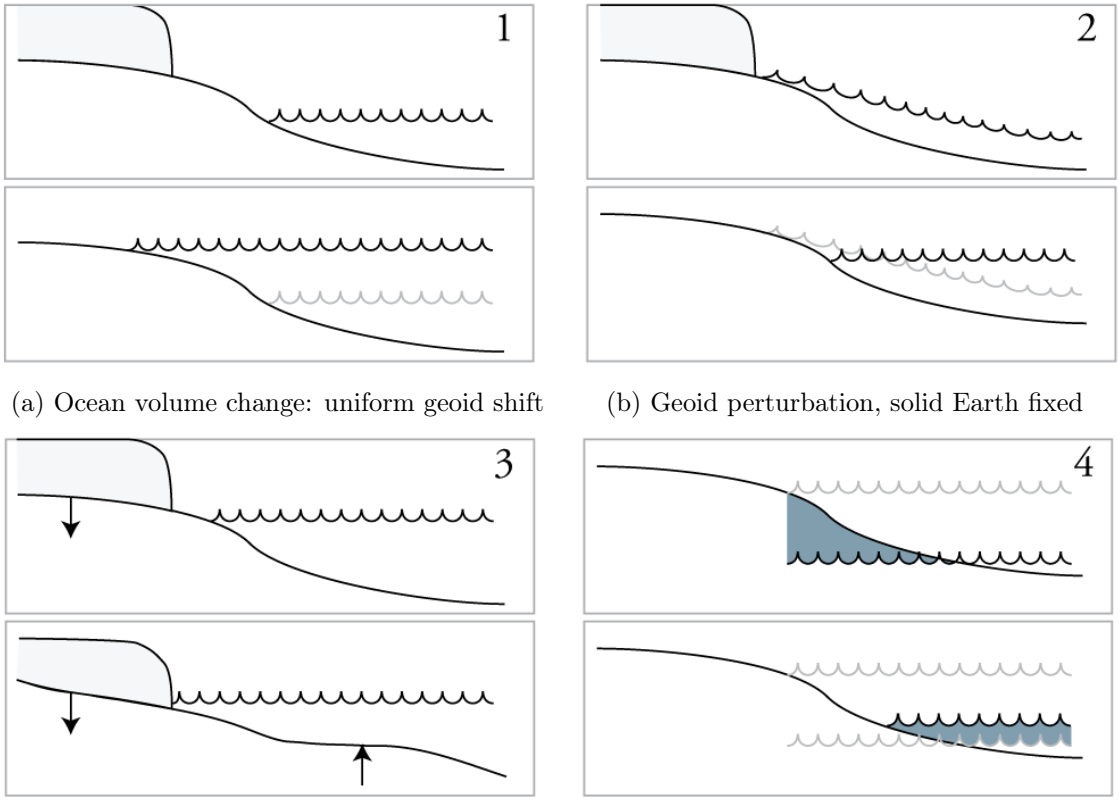

(a) Ocean volume change: uniform geoid shift

(b) Geoid perturbation, solid Earth fixed

(c) Solid Earth deformation

(d) Moving shorelines: shrunk ocean area

Figure 1.3: Graphical representation of the mechanisms described by the GSLE. Depicted are the solid Earth, the sea, and a shaded ice cap.

The goal in solving the GSLE is to find the change in solid Earth (ΔR_0) and geoid (ΔG_0) level at an initial time $t = 0$ such as 21 ka ago in comparison to the present. Note that this gives $\Delta R_0 - \Delta G_0 = \Delta T_0$, the change in topography compared to the present day. After guessing the initial conditions, the GSLE mechanisms and moving shoreline effect are used to calculate the intermediate solid Earth (ΔR_j), geoid (ΔG_j) and thus topography

(ΔT_j) changes, compared to the present. This is done in discrete time steps, using the change in ice cap volume as the forcing function. The last values calculated are ΔR_p, ΔG_p and ΔT_p at present time $t = p$. In a good model run, these values should be sufficiently low, as there should not be a topography difference between the calculated topography and the actual topography T_p. If it is classified as a misfit, a new guess of the solid Earth and geoid level at $t = 0$ is made, and the process repeats until a satisfactory match is found between the calculated and known present day topography. At this point, any topography at time $t = j$ can be calculated using:

$$T_j = T_p + \Delta T_j \tag{1.2}$$

Using the definition at equation (1.1), one can now distinguish land ($T_j \geq 0$) from sea ($T_j < 0$) at any time step.

Several methods exist to quantify the GSLE mechanisms and thus find ΔT_j. As only highly idealized situations (such as a non-deformable Earth) can be modeled algebraically, they must be solved using computer algorithms. The most used method is the pseudo-harmonic approach originally by Farrell and Clark (1976) and generalized by Kendall et al. (2005). This approach means most computations are done using spherical harmonics. Spherical harmonic functions represent surfaces that wrap around a sphere using combinations of complex sine and cosine functions. By choosing a right set of coefficients, any spatial function can be written as a sum of spherical harmonic functions. The advantage of using spherical harmonics is that they store variations up to the chosen harmonic degree with just a small set of coefficients. The disadvantage is that these models assume that the viscoelastic response is independent of position. This is not necessarily true, as the Earth is not homogeneous in temperature and chemical make-up, and therefore not homogeneous in mechanical properties (Spada et al., 2006). Yet, the pseudo-harmonic approach proves to give good fits to observations and there is a consensus among geophysicists on the functioning and correctness of the GSLE (Spada et al., 2011).

An important role is played by the forcing ice cap model. Such a model is created by geological observations, current day observations of land uplift and inverse solving of the GSLE (Peltier, 1994). The observations lead to a first educated guess for an ice cap model. The GSLE is solved with this ice cap model, and the misfits between calculated and measured RSL histories are determined. The ice model is adjusted accordingly, and this process iterates until misfits are minimized. Thus: the ice cap model is calibrated against a finite set of points, and can then be used to model the RSL everywhere. The currently most recent and used ice cap model is ICE-5G by Peltier (2004), that gives the ice cap thickness since 21 ka up to the present in steps of 1 ky.

Currently, the only open source sea level equation solver is SELEN 2.9 (Spada et al., 2012), which uses the pseudo-harmonic approach without applying the moving shorelines concept. As simulated by Kendall et al. (2005), this method creates vertical RSL misfits of up to 10% when comparing computed RSL histories with actual measurements. In tectonically

stable environments (no thrusting, subduction or moving blocks) the introduction of moving shorelines would bring these vertical misfits back to 1%.

1.3 Thesis aim

This research aims to contribute to statistical island biogeographic research in the area of the Aegean Sea by providing an accurate assessment of the changing area and isolation of islands in this sea. Biogeographic research such as published by Simaiakis et al. (2012) has led to large spatial databases of species and species variability in this region. A good assessment of the changing area and isolation of islands in the Aegean Sea as the RSL changes does however not exist currently. Earlier work by Lambeck (1996) on the RSL in the Aegean Sea has provided preliminary results specifically for archaeological purposes. The sea level equation solved in that research is however not a consistent 'moving shoreline' model such as provided by the GSLE, but a projection of the static sea level equation on the Aegean area. This thesis aims to improve this by using the GSLE to model RSL changes. It is also new in extracting the spatial statistics of size and isolation of islands after modeling the sea levels in this non-uniform way.

The research question of this thesis is: *How are island size and isolation in the Aegean Sea in the past 21 ka affected by relative sea level changes, taking into account surface loadings and gravitational effects?*

This research designs three steps to solve this question. In the first step the RSL will be modeled with moving shorelines. The results are expected to follow actual RSL measurements closely, which means a sea level rise of 40 meters is expected for the last 10 ky in most regions as seen in figure 1.1. Vertical errors of at maximum ± 20 meters may exist due to the tectonically active nature of the region (Stocchi, personal communication 17-5-2013). In the second step the calculated values of ΔT_j will be applied to a digital elevation model (DEM) with a resolution that is as high as possible. The old topography will be reclassified into two groups: land and sea. Due to the lower sea levels in the past, it is expected that both islands and the continent used to be larger than they are currently. In the third step the maps will be analyzed and the island size and isolation for 10 islands will be assessed for 10 islands using GIS procedures. Due to the originally lower sea levels, it is expected that islands in the past were bigger and closer to the continents and that these values change through time.

In chapter 2, a detailed description is provided of the method and definitions used to solve the above three research steps. Chapter 3 gives a short summary of the results. Chapter 4 discusses the implications, results and methodology. Chapter 5 concludes the thesis with a summary and and outlook for future research. The appendix at the end provides additional information on some of the steps taken, and will be referred to throughout the text.

Chapter 2

Methods

2.1 Solving the GSLE

2.1.1 Model set-up

The first step was solving the GSLE globally at a high spatial resolution. This was done by completely rewriting the GSLE solver of the Fortran 90 program SELEN 2.9 (Spada and Stocchi, 2007; Spada et al., 2012) to the GSLE with moving shorelines using parts of the numerical scheme provided in Kendall et al. (2005) and explained in appendix A. Already contained in SELEN was an equally spaced pixelation scheme from Tegmark (1996) and a method to decompose and synthesize spherical harmonic functions using the SHTOOLS library (Wieczorek, 2012). It also provided the interface to load any ice cap model and a method to compute the spherical harmonic deformation coefficients for any given viscoelastic Earth model.

A new Fortran routine was created to retrieve information from any given DEM for a given set of pixel coordinates. This routine relied on `gdallocationinfo` from the Geospatial Data Abstraction Library (Warmerdam, 2013).

Most loops were parallelized using the OpenMP scheme to use all available computational cores, and compilations were performed using the Intel Fortran Compiler `ifort` 13.1.1 for Linux 64 bit with an Intel i7 chip (Intel, 2013). Computation took approximately 8 hours when using 306252 pixels for spatial functions (four times as high as normal RSL simulations as e.g. Kendall et al. (2005) or Spada et al. (2012)) and up to spherical harmonic degree 256, set to be as high as fitting in the physical memory of the computer (twice the resolution of normal RSL simulations).

2.1.2 Data selection

The input required by the GSLE are a forcing ice cap model, a DEM and a viscoelastic Earth model. The forcing ice cap model implemented is the 10 arcminutes (0.167°) ICE-5G model by Peltier (2004) that was provided along with SELEN 2.9. It is calibrated to give best fits in both North America and Europe, which fits the study area of this research. The

DEM used was the DEMSRE3a, based on a combination of the SRTM 30+ (Becker et al., 2009) and ETOPO (Amante and Eakins, 2009) DEM with a resolution of 1/120 arcdegrees (0.00833°), with the WGS 84 geoid as datum (Hengl and Reuter, 2012). The viscoelastic Earth model is the VM2 Earth model with a lithosphere thickness of 90 km, as described in Peltier (2004) and Spada et al. (2012). This is the specific viscoelastic model used to create the ICE-5G model, hence a correct choice to use alongside the ice cap model. The simulation settings are summarized in table 2.1.

Table 2.1: Settings as used in GSLE simulation

Parameter	Setting	Source
Sampling resolution	306252 pixels	-
Spherical harmonic degree and order truncation level	256	-
Ice-cap model	ICE-5G	Peltier (2004)
DEM	DEMSRE3a	Becker et al. (2009); Amante and Eakins (2009); Hengl and Reuter (2012)
Viscoelastic Earth model	VM2 90km lithosphere	Peltier (2004); Spada et al. (2012)

2.2 Converting RSL data to paleo topography

After the RSL was calculated for all time steps, the next step was to convert the data to usable data in GIS software to assess the paleo (old) topography. The raw output of ΔT_j was extracted at a resolution of 0.1° for the Aegean Sea by decomposing the spherical harmonic function in a range of 32°–43°N and 16°–30°E using the spherical harmonics interface of SELEN. A small Fortran 90 program was written to extract this data from the database and convert it to ESRI ASCII grid format.

To find the topography at any given time step equation 1.2 ($T_j = T_p + \Delta T_j$) was used. For T_p the DEMSRE3a was used, for ΔT_j the raw program output was used. The difference in grid resolutions (0.0083°for the DEM, 0.1°for the extracted data) is of negligible influence, because the vertical DEM resolution was in integer steps of a meter, while the ΔT_j did not differ a full meter between adjacent grid cells. In other words: the neglected vertical differences in the DEM are greater than the neglected vertical differences in the extracted data. Hence, the full computation is $T_p + \Delta T_j = \text{DEM} + \text{extracted model output}$. This gridded addition was performed manually in Quantum GIS 1.8.0 (Quantum GIS development group, 2012) using *Raster* → *Raster calculator*.

The output thus contains the paleo topography in reference to the paleo sea levels, which means that everything with an elevation ≥ 0 is land, and everything below an elevation of 0 is water. This reclassification of values was performed within SAGA GIS (SAGA GIS

development group, 2011) using the module *Grid* → *Tools* → *Reclassify grid values*. Raster cells were given the number 1 for being greater or equal than 0, and given the number 0 for being below 0. This process was automated by applying these commands to all GeoTIFF files using the batch script in appendix B.1.

2.3 Island data extraction

To analyze the maps and the islands on them, it was necessary to have these maps in polygonized form and using an equal-area projected coordinate system to preserve areas, while using a Greek based projected coordinate system to minimize distance distortion. The areas were then extracted using Quantum GIS, while the distances were found using PostGIS (PostGIS Project Steering Committee, 2013). To speed up the process, the following work-flow was used:

1. The maps were transformed from regular projection to Lambert Azimuthal Equal-Area projection centered on Europe using `gdalwarp` and were then polygonized with `gdal_polygonize` (Warmerdam, 2013). The above operation was automated in batch mode to process all files directly, see appendix B.2.

2. 10 islands for which biotic data is available were selected by the owner of the Aegean species database Simaiakis (personal communication, 17-6-2013). See figure 2.1 for the selection.

3. The continental landmass and 10 islands were manually selected for all time steps and copied into unique layers, such that every layer contained 22 snapshots of one landmass.

4. The island size evolution through time is now easily found within Quantum GIS using the function *Vector* → *Geometry tools* → *Export/add geometry columns*. This calculates the area using the projected equal-area coordinate system.

5. The 11 vector layers containing the continent and 10 islands were warped to the WGS84 / Greek Grid projected coordinate system using `gdalwarp` in batch mode as in step 1.

6. The shapefiles were loaded into PostGIS. Using the built-in shortest distance calculator the distances were determined between island shapefiles and the closest large landmass, see table 2.2. See appendix B.3 for the query.

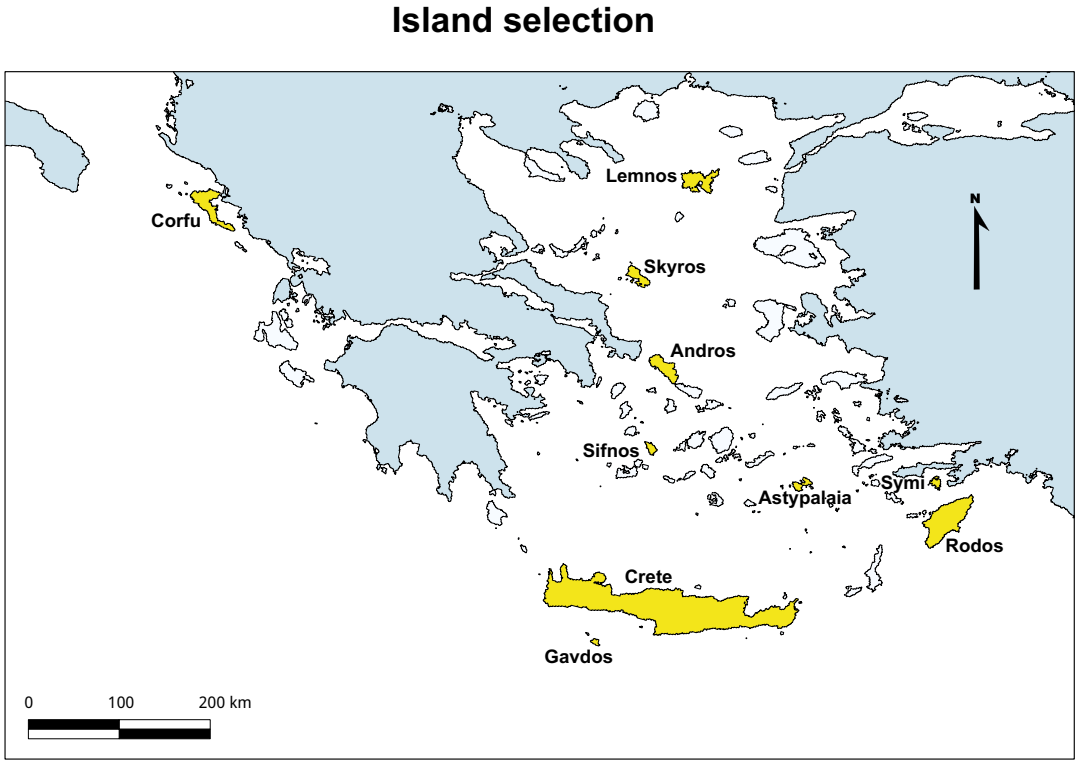

Figure 2.1: Selected islands for the island configuration study drawn in yellow and annotated. The present day continental landmass has been shaded with dark blue.

Table 2.2: Island selection information and most representative definition of 'isolation' from Simaiakis, personal communication 17-6-2013.

Island	**Present day area [km^2]**	**Isolation from**
Andros	381	Continent
Astypalaia	96	Continent
Corfu	614	Continent
Crete	8265	Continent
Gavdos	33	Crete
Lemnos	476	Continent
Rodos	1408	Continent
Sifnos	77	Continent
Skyros	207	Continent
Symi	67	Continent

Chapter 3

Results

3.1 Paleo topography in the Aegean area

After running the program, the modeled topography change from time $t = j$ up to the present, thus $-\Delta T_j$, can be projected onto a present day shoreline map. A selection of 4 time steps is presented in figure 3.1. In oceanic areas this shows the sea levels relative to the present day sea topography: the RSL. More generally, it depicts the change of the datum (0 elevation) through the entire Aegean region relative to the present datum. It indicates that sea levels were down by 145 meters 21 ka ago. The RSL change becomes bigger at greater distances from land, as these regions subsided the most due to the loading effect of the increasing sea water mass. The RSL at 11 ka is at its maximum only 43 meters below the present day sea level, which means the sea level rose more rapidly in the period from 21 ka to 11 ka than it rose from 11 ka to the present. The datum difference has also been projected onto the present day DEM for 4 time steps to provide better insight into the vertical scale of the RSL in comparison to the differences in DEM, see figure 3.2. An example of the reclassified topography into land and water is given in figure 3.3.

3.2 Island configuration statistics

The changing area and shortest distance to a large landmass of 10 islands were found using Quantum GIS, respectively PostGIS. These values were plotted and can be found in figures C.1-C.3 on pages 39-41. Four examples, from the east, north, central and south Aegean area, are given and annotated along with a map on figures 3.4-3.11. They serve to give insight in the different ways island configurations have changed and how this can be seen in the graphs.

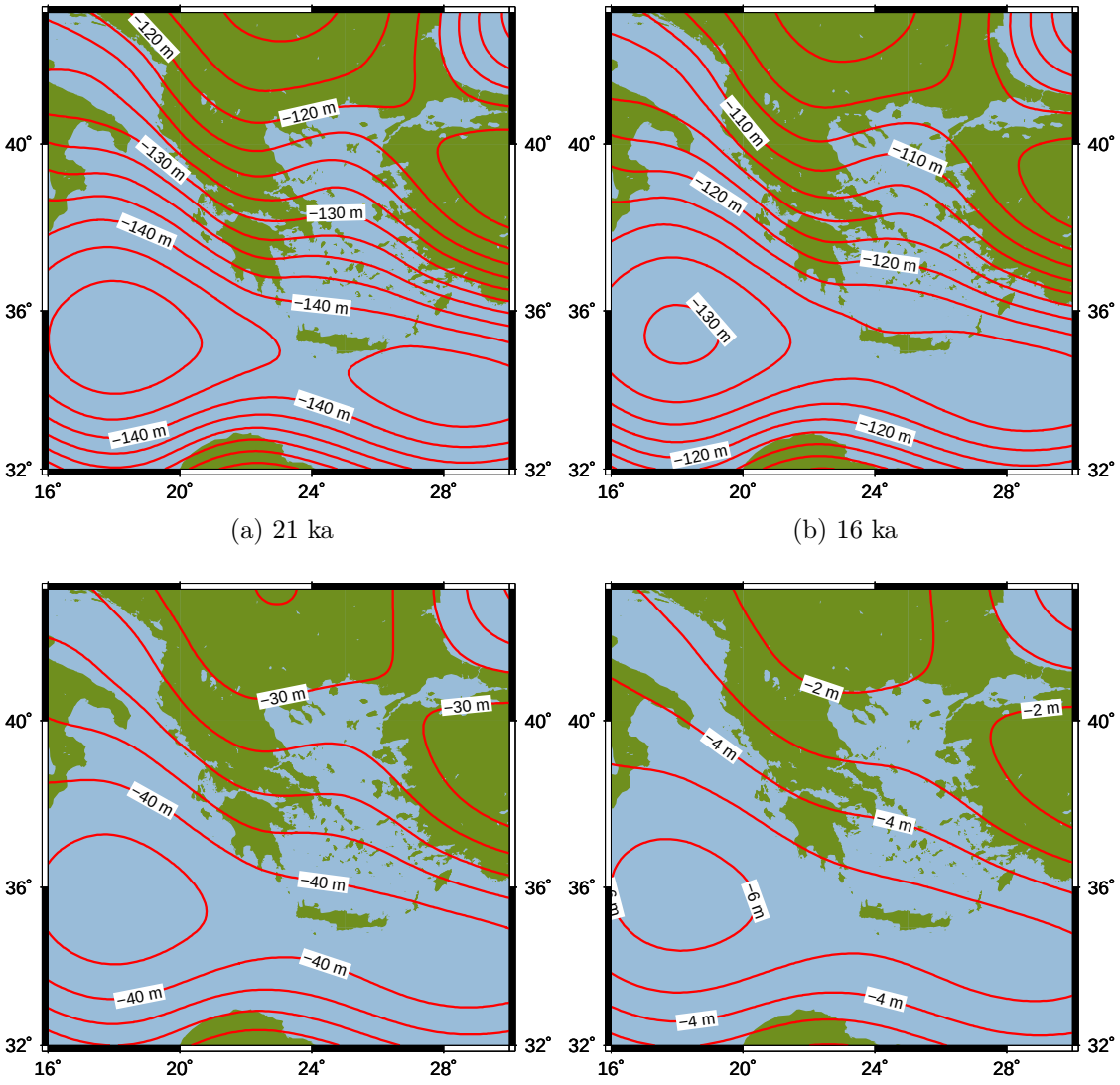

(a) 21 ka

(b) 16 ka

(c) 11 ka

(d) 6 ka

Figure 3.1: Predicted datum difference relative to the current datum in the Aegean area for selected time steps using the GSLE. This shows the sea levels relative to the current day sea levels in oceanic areas. The data is projected onto a present day shoreline map by Wessel and Smith (1996).

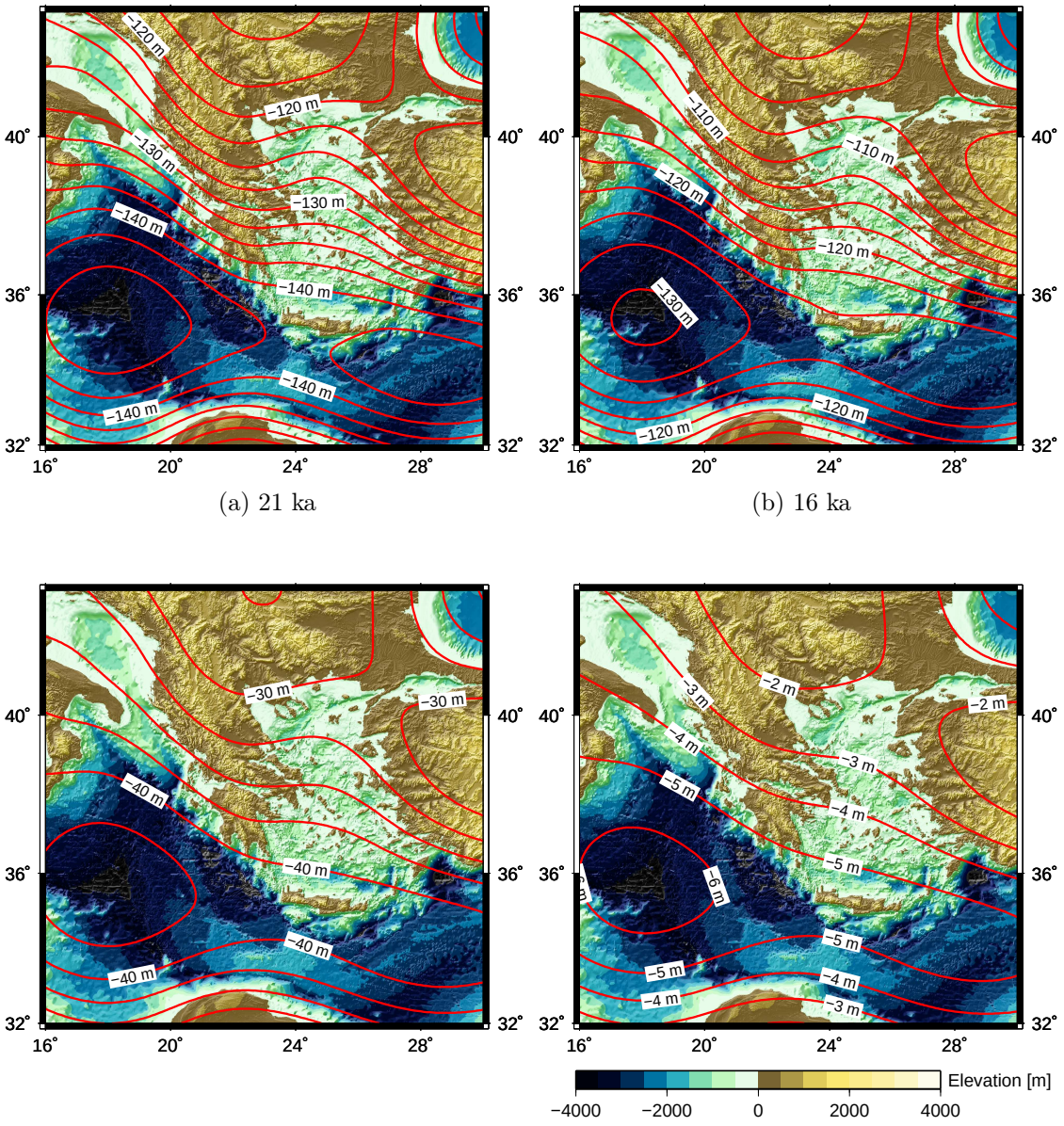

(a) 21 ka (b) 16 ka

(c) 11 ka (d) 6 ka

Figure 3.2: Predicted datum difference relative to the present day datum in the Aegean area for selected time steps using the GSLE. Data is projected onto present day WGS 84 based DEM by Hengl and Reuter (2012).

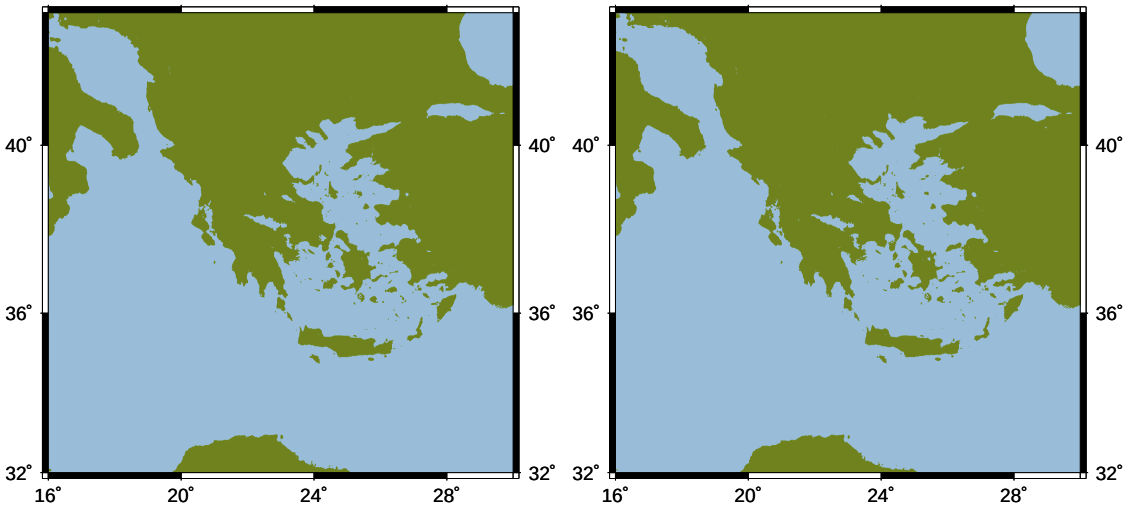

(a) 21 ka

(b) 16 ka

(c) 11 ka

(d) 6 ka

Figure 3.3: Predicted land surface obtained through solving the GSLE for selected time steps.

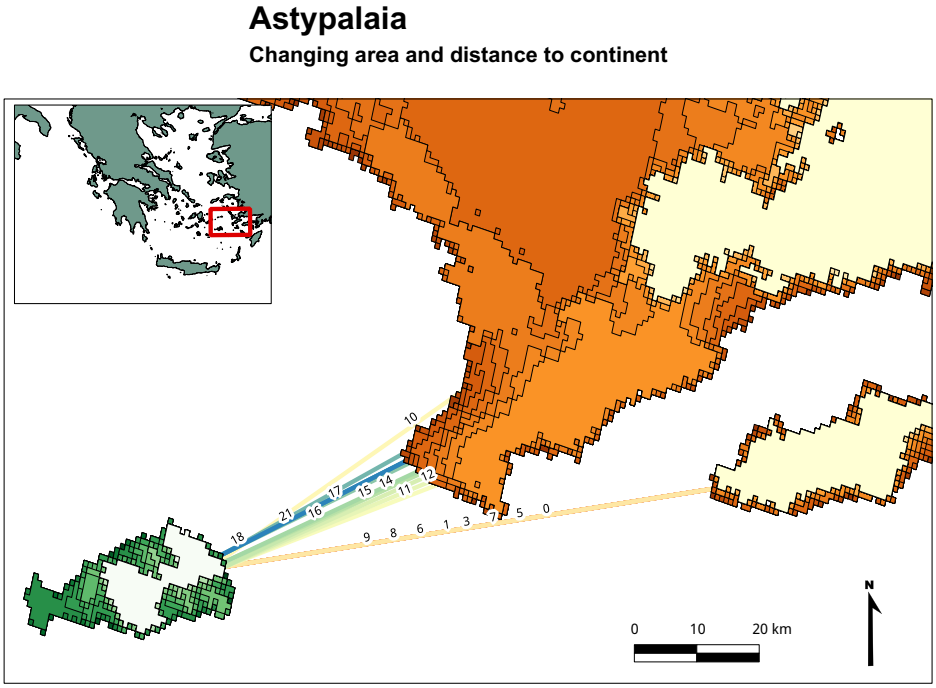

Figure 3.4: The area and isolation of Astypalaia as modeled with the GSLE. The shortest distance between the island and continent is projected on the map along with a label that denotes the time in ka for which this shortest distance applies. All other islands have been omitted for clarity. Darker colors represent older land configurations.

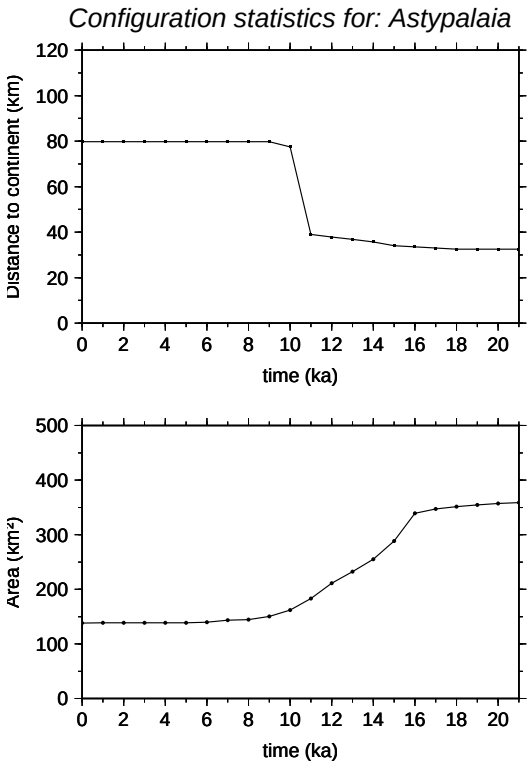

Figure 3.5: The area and isolation through time of Astypalaia as modeled with the GSLE.

The first example, Astypalaia, is located in the east Aegean area. The distance to the continent at 21 ka used to be about 40 km, not because the island surface laid closer to the continent, but because the continental landmass used to surface closer to Astypalaia. The distance doubled from about 40 to 80 km at 10 ka, because the continent reduced in size rapidly. The island its area was roughly twice its current size. At about 10 ka both the area and isolation remained steady at their present day levels.

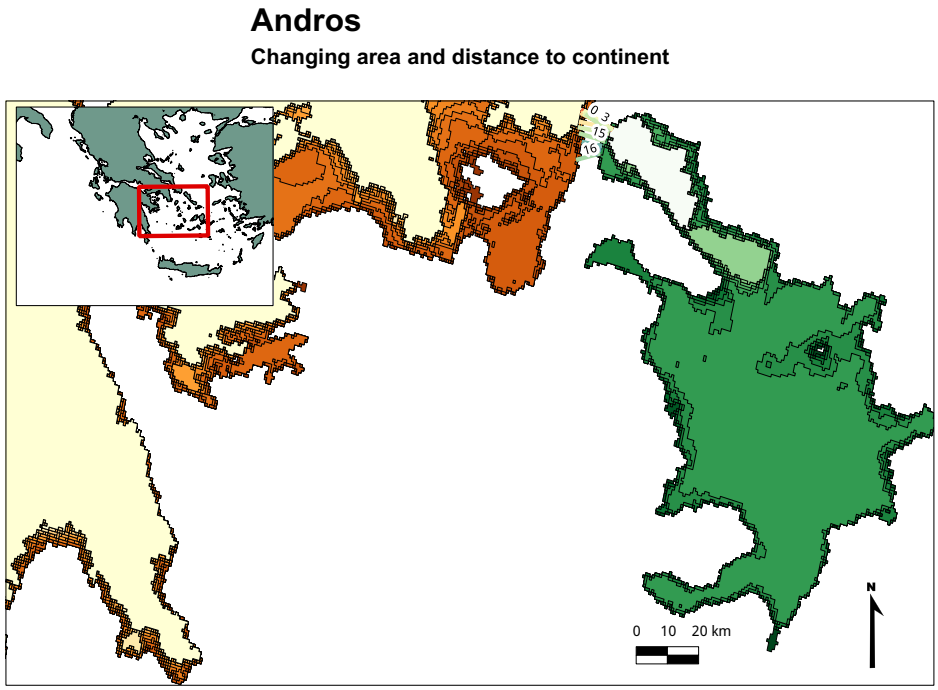

Figure 3.6: The area and isolation of Andros as modeled with the GSLE. The shortest distance between the island and continent is projected on the map along with a label that denotes the time in ka for which this shortest distance applies. All other islands have been omitted for clarity. Darker colors represent older land configurations.

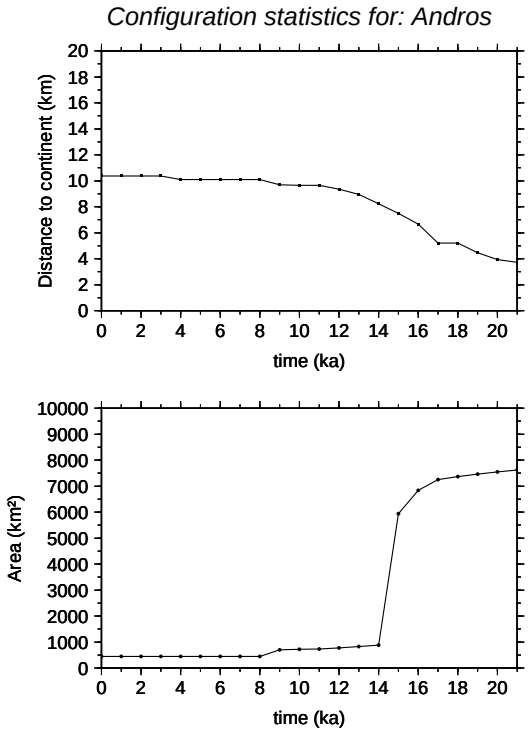

Figure 3.7: The area and isolation through time of Andros as modeled with the GSLE.

The second example, Andros, is located in the central Aegean area. It experienced little change in distance, rising steadily from 4 km at 21 ka to its present day distance. The area, however, was about 15 times as high at 21 ka when it was connected to other islands in the east Cyclades. At 14 ka it rapidly decreases in size towards current values.

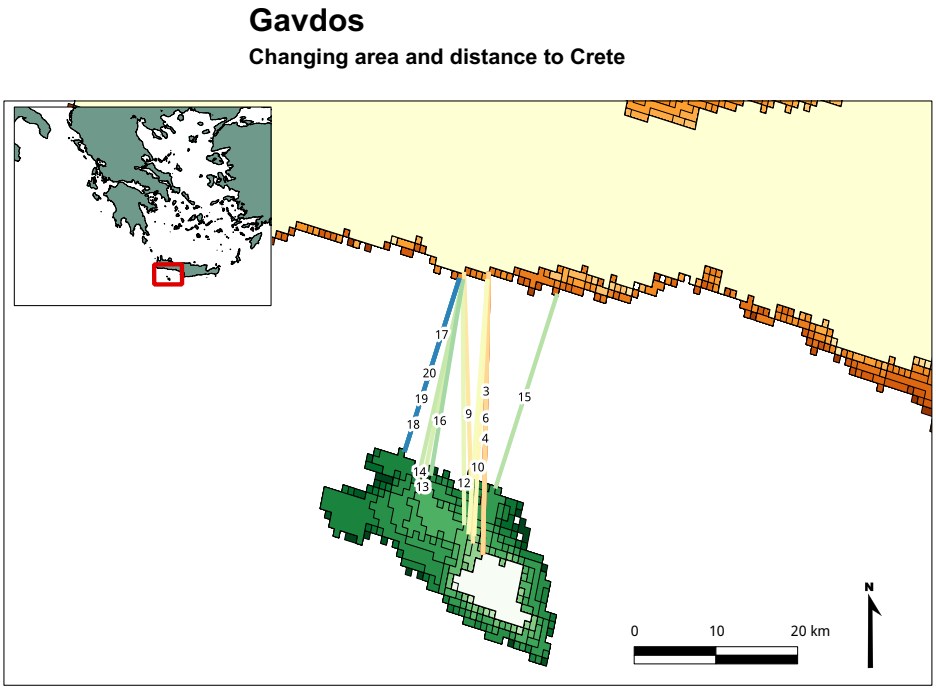

Figure 3.8: The area and isolation of Gavdos as modeled with the GSLE. The shortest distance between the island and continent is projected on the map along with a label that denotes the time in ka for which this shortest distance applies. Darker colors represent older land configurations.

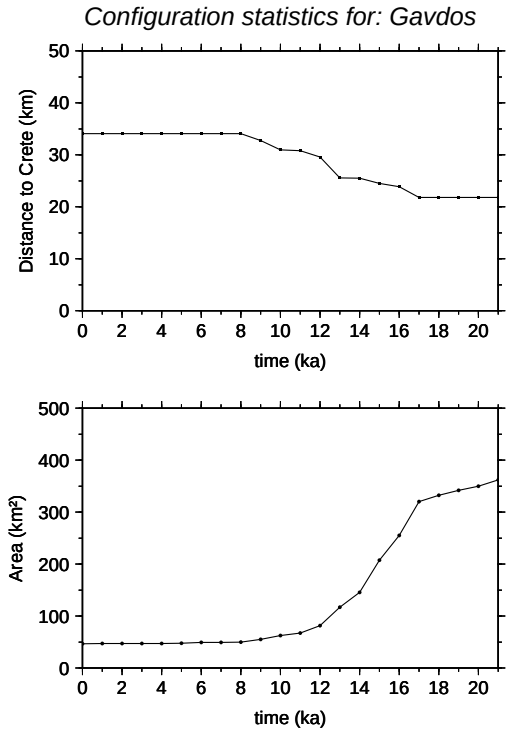

Figure 3.9: The area and isolation through time of Gavdos as modeled with the GSLE.

The third example, Gavdos, is located in the south Aegean area. The distance to Crete at 21 ka is almost half of that today, mostly because the edge of Gavdos was located closer to Crete at earlier times. The area was about 7 times as high at 21 ka. At about 8 ka both the area and isolation remain steady at their present day levels.

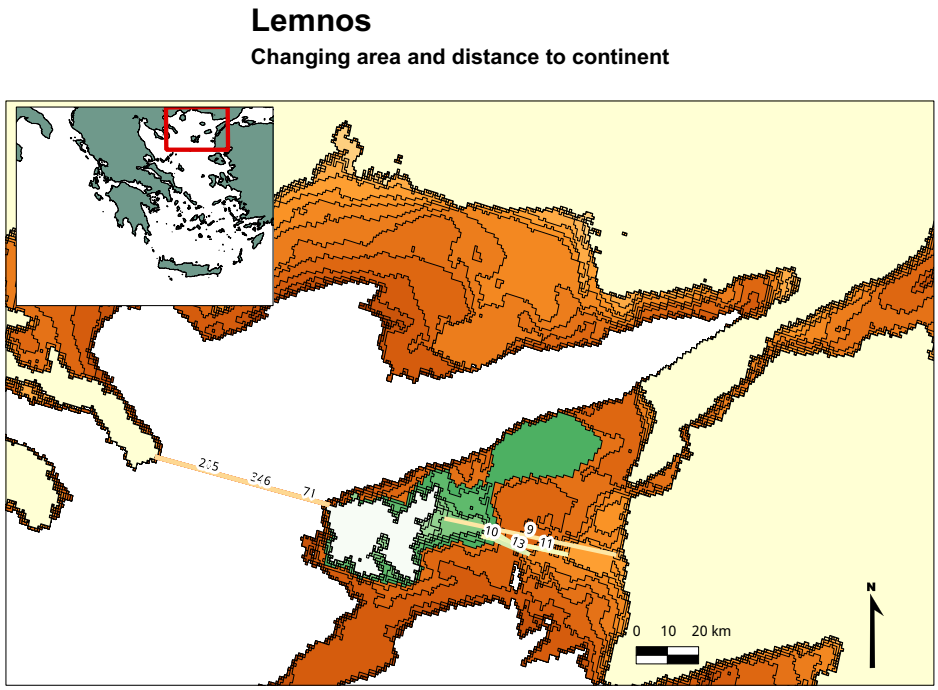

Figure 3.10: The area and isolation of Lemnos as modeled with the GSLE. The shortest distance between the island and continent is projected on the map along with a label that denotes the time in ka for which this shortest distance applies. All other islands have been omitted for clarity. Darker colors represent older land configurations.

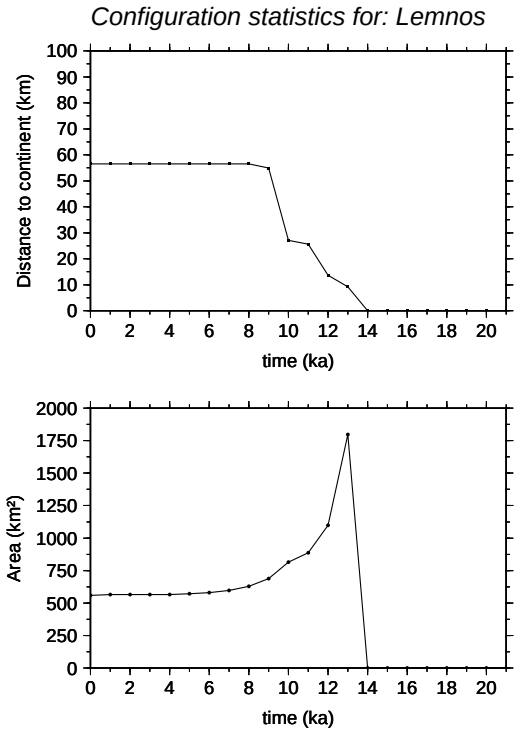

Figure 3.11: The area and isolation through time of Lemnos as modeled with the GSLE.

The fourth example, Lemnos, is located in the north Aegean area. This island is fully connected to the continent until 13 ka, when it detaches. The island then takes the configuration it has today at roughly 9 ka.

Chapter 4

Discussion

4.1 Interpretation and implications of the results

The island configurations through time show a unique decrease in area and increase in isolation per island. Four trends are found in the results. The first is found for Gavdos, which used to surface closer to Crete than it does now, thus was larger and less isolated. The second trend is found for Astypalaia, Rodos and Symi, which were less isolated because the continental landmass itself surfaced closer to these islands. The third trend is seen for Andros, Skyros and Crete, which did not see much isolation change but were 25-1500% larger than currently. The fourth trend is seen for Corfu and Lemnos, which were connected to the continent up to 13, respectively 14 ka.

The theory of island biogeography predicts that all islands used to be more biodiverse than they are at present, because of the increased areas and decreased isolation. The theory therefore predicts that RSL rise has had biogeographic repercussions on the biodiversity on these islands. Such a hypothesis must be tested by statistical biogeographic research.

4.2 Methodological discussion

Some remarks can be made about the results. The found values of the RSL at 10 ka are close to -40 meters as was predicted using figure 1.1. The values are also in the same range as the global RSL as used in earlier research by Norder (2012), and alike those as found by Lambeck (1996). This does not mean the modeled RSL is in accordance with the actual RSL changes in the Aegean area. The main reasons for possible deviations are the resolution, correctness and handling of input data, and the disregard for external processes.

The input data of the GSLE were the ice cap model, the viscoelastic Earth model and the DEM. The ice cap model ICE-5G had a low spatial resolution at $0.167°$. Despite not being very precise, the ice caps were located outside of the study area. The mechanisms were therefore only dependent on distance and not on the spatial resolution. The correctness of the model is assumed since it is constructed specifically to reduce misfits in North America and Europe, which includes the studied area. The ice cap model is assumed to be applied

correctly and not a source of errors as it was designed to reduce misfits between predictions and measurements.

The symmetric viscoelastic Earth model VM2 was designed alongside ICE-5G, thus its use alongside ICE-5G should also reduce misfits. Yet, it is doubtful that it applies to the tectonically active Aegean region for the subsurface around a subduction setting is very heterogeneous in make-up. Despite this fact, the pseudo-spectral approach only allows for a symmetric response model. To solve the GSLE, VM2 was the best candidate at hand. Finite elements simulations may create better heterogeneous Earth models.

The DEM used, DEMSRE3a, had a spatial resolution of 0.00833°. The vertical resolution was in integers of 1 meter only. A higher vertical DEM resolution would not have made the results more accurate, for processes like tides have been neglected which could create variations on a 1 meter scale as well. Sampling the DEM in the program could be improved. Every sampled pixel represented roughly 1000 pixels from the DEM, or 30×30 km. This could lead to random errors as a single pixel sampled that is above sea suddenly represents 1000 pixels above sea. However, it is assumed that the effect of these random errors has little influence because the model still sampled at a high resolution (306252 pixels) compared to the surface of the Earth.

The calculations of *present day* island area generally gave too large sizes by up to 50% for islands of less than a 100 km^2. This is caused by the DEM giving any pixel with a shoreline the maximum, rather than the mean, elevation within that pixel. Every island is therefore completely outlined by pixels, as can be seen on figure C.4 on page 42. This means that islands with a large perimeter compared to their present size (which is the case for small and long islands) gather a lot of extra area around their perimeter. This error might not be present in paleo area reconstructions, because it gives the mean rather than the maximum elevation in other pixels. At any rate, the results can be used to check for order of magnitude changes, which are often larger than the 50% error.

The calculations of the isolation in the present day give correct values with an error of about -1 km, which was expected considering figure C.4. Because landmasses are all outlined by pixels, the calculated distance between two landmasses will be between 0–2 km too short. It remains a question whether 'isolation' is truly captured in a single number of the distance between island and a large landmass. A series of islands near the continent could function as 'stepping stones' for biota, such that they could cross large distances by inhabiting intermediate islands as well.

4.3 External processes

Secondly, two external processes may have played a role that were neglected. These were the correction for grounded ice and tectonics. The correction for grounded ice means the ocean area is reduced when ice caps are so large that they touch the ground – at such points no fluid water can be present. This part may be added into the GSLE solver as proposed by Kendall et al. (2005). The effects of this are assumed to be of no influence for

the past 10 ka when there was no grounded ice present in ICE-5G.

An important but lacking feature in this model is correcting for tectonics. The Aegean area is tectonically active with fault zones and volcanism. Although Stocchi (personal communication, 17-5-2013) noted these effects may be as high as ±20 meters at 21 ka ago, that is an absolute upper limit on the tectonic speeds. However, as showed in figure 1.1, an instantaneous sea level drop of 8 meters at 1.5 ka is most likely explained as movement along a fault. To incorporate these effects, one must study the tectonic movements of *all* the islands involved individually. This could for example be done by geological research of raised beaches and local RSL measurements, or a literature review of such research.

Chapter 5

Conclusion

5.1 Summary

The theory of island biogeography states that island size and isolation from other landmasses are the main controlling factors on the number and kind of island species. On a time scale of tens of thousands of years this island configuration (i.e. size and isolation) is not static but changes along with sea level variations relative to the landmass. Recent statistical biogeographic research used global mean sea level variations to assess the influence of changing island configurations. Sea level change since the last glacial maximum (21.000 years ago, abbreviated to 21 ka) has been induced by the melting of ice caps. Beside the uniform sea level rise caused by the volume exchange of water from ice caps to oceanic basins, the redistribution of mass affects the Earth its gravity field, thus also the sea surface level, and causes the solid Earth to deform under the new surface load distribution, changing land relative to sea levels (as shown in 1.3). The three mechanisms cause the relative sea level (RSL) to change in a non-uniform way around the world. To correctly study island biodiversity through time in an area, one must thus not use the global mean RSL change, but use RSL variations in both time *and* space. To describe RSL variations a sea level equation was proposed by Woodward (1888) and Farrell and Clark (1976). The theory was later extended to the generalized sea level equation (GSLE) by Mitrovica and Milne (2003) that realistically models shrinking ocean areas as sea levels drop and shorelines migrate seawards. Applying the GSLE might thus lead to a better assessment of the changing island configuration through time for more accurate statistical island biogeographic research.

This thesis focused on modeling the changing island configurations in the Aegean area (Greece, Southeast Europe), to aid biogeographical work that studies species distributions in the region. This thesis improves on earlier models by applying the GSLE, and is new in assessing the island configurations in the Aegean Sea. The research question was: *How are island size and isolation in the Aegean Sea in the past 21 ka affected by relative sea level changes, taking into account surface loadings and gravitational effects?*

To answer the research question a model of the changing RSL in the Aegean Sea through time has been developed by applying the GSLE for the last 21 ka. Island size and isolation

were then extracted for 10 islands. The method correctly finds the present distance to the continent, but overestimates the area by up to 50%. It also does not involve tectonics which might play an important role for islands in the Aegean Sea. Despite not being fully correct, it already provides a more accurate assessment of changing island configurations than by using global mean RSL changes. Further improvements on the model can be made using a better DEM, simulate on a higher resolution and incorporate tectonics. The gathered data can be used island biogeographical statistical research of species variability in the Aegean Sea.

Four trends are identified in the results. The first two are islands that were less isolated because they surfaced closer to the other landmass (Gavdos) or because the continent itself surfaced closer to the islands (Astypalaia, Rodos and Symi). The second two are islands that did not see isolation change but large area change (Andros, Skyros and Crete) and islands that were completely connected to the continent (Corfu until 13 ka, Lemnos until 14 ka).

5.2 Outlook

The gathered data can be used in a biogeographic study of these 10 islands in the Aegean Sea. By following the outlined method the island configuration for any island, in the Aegean Sea or elsewhere, can be assessed.

The theory of island biogeography can be used to predict that islands with large changes in area or isolation witnessed large biogeographic events such as extinctions or endemisation of species. The results of this thesis show two areas in the Aegean Sea that experienced large changes in area or isolation. The east Cyclades islands all used to be connected to each other at 21 ka, but were at no moment connected to the continent. The east Aegean islands such as Lesbos used to be completely connected to the continent for an extended period of time, several were connected to each other. Both areas serve as interesting cases to test a dynamic theory of island biogeography since it predicts that the connections must have left biodiverse traces on all the islands involved.

Acknowledgements

I would like to express my gratitude to a number of people that have helped me a lot during the process of researching and writing this thesis. First of all my supervisor Kenneth Rijsdijk, from the Institute of Biodiversity and Ecosystem Dynamics at the Universiteit van Amsterdam in the Netherlands, for his enthusiasm and ability to make me interested in such a field as biogeography! The involved supervision pushed me to delve deeply into all the individual disciplines involved in this research and made me appreciate the amount of revolutionary interdisciplinary research that can still be done. As Paolo Stocchi, connected to the Royal Netherlands Institute for Sea Research (NIOZ), told me when I asked why so little research existed on paleo island configurations: "Geophysicists just don't care"! I want to thank Paolo Stocchi for the helpful brief course he gave on the physical and methodological workings of the GSLE, and how I could update SELEN 2.9 to include the GSLE. I want to thank Giorgio Spada, from the Università degli Studi di Urbino in Italy, for releasing SELEN 2.9 in its open source and well documented format. Also many thanks for inspiring me to adapt SELEN to the GSLE scheme, by saying "it is not so difficult after all". I want to thank Stylianos Simaiakis, from the University of Crete in Greece, for the enthusiasm he has shown for the results. His comparisons of calculations versus actual data made me rethink all the steps I took to arrive at my calculated results, which helped me to understand why reality was not conforming to my results. Often I turned out to be the one that was wrong.

Also I want to thank my family and friends for bearing with me all the time I was working on or could not stop talking my thesis. Your support has been awesome!

Bibliography

Amante, C. and Eakins, B. (2009). ETOPO1, 1 Arc-Minute Global Relief Model: Procedures, Data Sources and Analysis. Technical report, NOAA Technical Memorandum NESDIS NGDC-2.

Becker, J., Sandwell, D., Smith, W., Braud, J., Binder, B., Depner, J., Fabre, D., Factor, J., Ingalls, S., Kim, S., Ladner, R., Marks, K., Pharaoh, A., Trimmer, R., Von Rosenberg, J., Wallace, G., and Weatherall, P. (2009). Global bathymetry and elevation data at 30 arc seconds resolution: SRTM30_PLUS. *Marine Geodesy*, 32, 355–371.

Douglas, B., Kearney, M., Leatherman, S., et al. (2001). Sea level rise: history and consequences. *International Geophysics Series*, 75, 1–232.

ESRI (2013). World imagery. Available within ArcGIS and from `http://www.arcgis.com/home/item.html?id=10df2279f9684e4a9f6a7f08febac2a9`.

Farrell, W. and Clark, J. A. (1976). On postglacial sea level. *Geophysical Journal of the Royal Astronomical Society*, 46, 647–667.

Hengl, T. and Reuter, H. (2012). Global Relief Model based on SRTM 30+ and ETOPO DEM at 1/120 arcdeegres. Retrieved May 2nd, 2013, from `http://worldgrids.org/doku.php?id=wiki:demsre3`.

Intel (2013). Ifort 13.1.1 20130313 [Fortran 90 compiler]. Available from `http://software.intel.com/en-us/non-commercial-software-development`.

Kendall, R. A., Mitrovica, J. X., and Milne, G. A. (2005). On post-glacial sea level–II. Numerical formulation and comparative results on spherically symmetric models. *Geophysical Journal International*, 161, 679–706.

Lambeck, K. (1996). Sea-level change and shore-line evolution in Aegean Greece since Upper Palaeolithic time. *Antiquity*, 70, 588–611.

Lambeck, K. and Chappell, J. (2001). Sea level change through the last glacial cycle. *Science*, 292, 679–686.

MacArthur, R. H. and Wilson, E. O. (1963). An equilibrium theory of insular zoogeography. *Evolution*, 17, 373–387.

Milne, G. A., Mitrovica, J. X., and Davis, J. L. (1999). Near-field hydro-isostasy: the implementation of a revised sea-level equation. *Geophysical Journal International*, 139, 464–482.

Mitrovica, J. X. and Milne, G. A. (2003). On post-glacial sea level: I. general theory. *Geophysical Journal International*, 154, 253–267.

Norder, S. J. (2012). The influence of sea level fluctuations and land use patterns on oceanic island biodiversity; A biogeographic comparison of gastropod species diversity on eight oceanic island archipelagos. Master's thesis, Universiteit van Amsterdam, the Netherlands. 63 pages.

Paulay, G. (1994). Biodiversity on oceanic islands: its origin and extinction. *American Zoologist*, 34, 134–144.

Peltier, W. (1974). The impulse response of a Maxwell Earth. *Reviews of Geophysics*, 12, 649–669.

Peltier, W. (2004). Global glacial isostasy and the surface of the ice-age Earth: The ICE-5G (VM2) model and GRACE. *Annual Review of Earth and Planetary Sciences*, 32, 111–149.

Peltier, W. R. (1994). Ice age paleotopography. *Science*, 265, 195–201.

Pluet, J. and Pirazzoli, P. (1991). *World atlas of Holocene sea-level changes*, volume 58. Elsevier Science, Amsterdam, the Netherlands. 300 pages.

PostGIS Project Steering Committee (2013). PostGIS 9.2.4-1 [GIS database]. Available from `http://postgis.net/`.

Quantum GIS development group (2012). Quantum GIS 1.8.0-1 [GIS software]. Available from `http://qgis.org/`.

SAGA GIS development group (2011). SAGA GIS 2.0.7 [GIS software]. Available from `http://www.saga-gis.org/`.

Simaiakis, S. M., Tjørve, E., Gentile, G., Minelli, A., and Mylonas, M. (2012). The species–area relationship in centipedes (Myriapoda: Chilopoda): a comparison between Mediterranean island groups. *Biological Journal of the Linnean Society*, 105, 146–159.

Spada, G., Antonioli, A., Cianetti, S., and Giunchi, C. (2006). Glacial isostatic adjustment and relative sea-level changes: the role of lithospheric and upper mantle heterogeneities in a 3-D spherical Earth. *Geophysical Journal International*, 165, 692–702.

Spada, G., Barletta, V., Klemann, V., Riva, R., Martinec, Z., Gasperini, P., Lund, B., Wolf, D., Vermeersen, L., and King, M. (2011). A benchmark study for glacial isostatic adjustment codes. *Geophysical Journal International*, 185, 106–132.

Spada, G., Melini, D., Galassi, G., and Colleoni, F. (2012). Modeling sea level changes and geodetic variations by glacial isostasy: the improved SELEN code. *ArXiv e-prints*. Retrieved from `http://arxiv.org/abs/1212.5061`.

Spada, G. and Stocchi, P. (2007). SELEN: A Fortran 90 program for solving the "sea-level equation". *Computers & Geosciences*, 33, 538–562.

Tegmark, M. (1996). An icosahedron-based method for pixelizing the celestial sphere. *The Astrophysical Journal*, 470, L81–L84.

Warmerdam, F. (2013). GDAL 1.10.0 [Library]. Available from `http://www.gdal.org/`.

Wessel, P. and Smith, W. H. (1996). A global, self-consistent, hierarchical, high-resolution shoreline database. *Journal of Geophysical Research*, 101, 8741–8743.

Whittaker, R. J. and Fernández-Palacios, J. M. (2006). *Island biogeography: ecology, evolution, and conservation*. Oxford University Press. 430 pages.

Whittaker, R. J., Triantis, K. A., and Ladle, R. J. (2008). A general dynamic theory of oceanic island biogeography. *Journal of Biogeography*, 35, 977–994.

Wieczorek, M. (2012). SHTOOLS 2.8 [Fortran 90 library]. Available from `http://shtools.ipgp.fr/`.

Woodward, R. S. (1888). On the form and position of mean sea level. *Geological Survey Bulletin of the United States*, 48, 87–170.

Appendix A

Solving the pseudo-spectral GSLE

A short description of the generalized sea level equation (GSLE) is given below. Topography T was defined as the distance of the solid Earth R over the geoid G. Within the theory of the GSLE it is more common to turn this definition around, and one describes the sea depth SD with:

$$SD(\omega, t_j) = -T(\omega, t_j) = G(\omega, t_j) - R(\omega, t_j). \tag{A.1}$$

A positive number now denotes the bathymetry, a negative number the topography. This can be seen in figure 1.2.

By choosing t_0 before t_j, one can express G and R in reference to $t = 0$,

$$\begin{aligned} G(\omega, t_j) &= G(\omega, t_0) + \Delta G(\omega, t_j) \\ R(\omega, t_j) &= R(\omega, t_0) + \Delta R(\omega, t_j) \end{aligned} \tag{A.2}$$

and substitution gives

$$\begin{aligned} SD(\omega, t_j) &= \underbrace{G(\omega, t_0) - R(\omega, t_0)} + \underbrace{\Delta G(\omega, t_j) - \Delta R(\omega, t_j)} \\ &= \qquad SD(\omega, t_0) \qquad + \qquad \Delta SD(\omega, t_j)\ . \end{aligned} \tag{A.3}$$

To find only the present depth of the water, and not the topography, one can multiply SD by an 'ocean function' that cancels out all positions where the solid Earth rises above the sea level. This method essentially entails to *project* the sea depth SD on the ocean area only, see also figure 1.2.

$$S(\omega, t_j) = SD(\omega, t_j) \cdot C(\omega, t_j) \tag{A.4}$$

where

$$C = \begin{cases} 1 & \text{if } SD(\omega, t_j) > 0 \\ 0 & \text{if } SD(\omega, t_j) \leq 0 \end{cases}. \tag{A.5}$$

Substitute equation (A.3) in equation (A.4) to write:

$$S(\omega, t_j) = \big(SD(\omega, t_0) + \Delta SD(\omega, t_j)\big) \cdot C(\omega, t_j) \tag{A.6}$$

If one then tries to write the sea depth in analogy to (A.3) as a reference state plus a deviation, one finds another way to write (A.6):

$$S(\omega, t_j) = S(\omega, t_0) + \Delta S(\omega, t_j) = SD(\omega, t_0) \cdot C(\omega, t_0) + \Delta S(\omega, t_j) \tag{A.7}$$

By equating (A.6) and (A.7), one can derive an expression for ΔS, the change in observed sea level depths, that Kendall et al. (2005) dub the generalized sea level equation (GSLE):

$$\begin{aligned} \Delta S(\omega, t_j) &= SD(\omega, t_0) \cdot C(\omega, t_j) + \Delta SD(\omega, t_j) \cdot C(\omega, t_j) - SD(\omega, t_0) \cdot C(\omega, t_0) \\ &= \underbrace{\Delta SD(\omega, t_j) \cdot C(\omega, t_j)}_{\text{RSL change on present ocean area}} + \underbrace{SD(\omega, t_0) \cdot (C(\omega, t_j) - C(\omega, t_0))}_{\text{redistributed water as ocean area changed}} \end{aligned} \tag{A.8}$$

This equation indicates that the change in present sea depth S equals the change of sea depth ($\Delta SD(\omega, t_j)$) on the ocean area at time $t = j$, with a correction for the redistribution of the water that was already present, as the rise and fall of sea level shrink or enlarge the ocean area. This equation is an integral equation because a change in RSL influences the geoid and solid Earth deformation (due to changing the mass and loading at that point) – which in turn influences the RSL that is to occur at that point through $\Delta SD(\omega, t_j) = \Delta G - \Delta R$ and the ocean function $C(\omega, t_j)$. It must be noted that the GSLE cannot be solved for a single region alone, as every change of sea level affects the sea levels around it. It must thus be solved globally.

Using the generalized sea level equation (GSLE) with an explicit expression for $\Delta S(\omega, t_j)$ as found in section 1.2 and equation (A.8), the equation can be rewritten to give the change between two time steps rather than the change from the beginning:

$$\begin{aligned} \delta S(\omega, t_j) &= \Delta S(\omega, t_j) - \Delta S(\omega, t_{j-1}) \\ &= \Delta SD(\omega, t_j) \cdot C(\omega, t_j) + SD(\omega, t_0) \cdot (C(\omega, t_j) - C(\omega, t_0)) - \Delta S(\omega, t_{j-1}) \end{aligned} \tag{A.9}$$

which will be the method used to solve the GSLE through time. It can be noted that cf. equation (A.1) and figure 1.2, SD is the negative topography. We can thus substitute $SD_0 = -T_0$. The explicit dependence on location (ω) will be dropped, and time will be denotated with a subcript.

$$\delta S_j = \Delta SD_j C_j - T_0(C_j - C_0) - \Delta S_{j-1} \tag{A.10}$$

The topography at T_0 is not yet known, but the present day topography T_p is known. We can thus write $T_0 = T_p - \Delta SD_j$, or $T_p = T_0 + \Delta SD_j$. The goal in solving the GSLE is to

find a value for T_0 and ΔSD_j that returns the present day topography. In other words: the GSLE is solved when the 'guessed' initial conditions at $t = t_0$ lead to the present day topography, using the forcing ice cap function.

The iteration scheme from Kendall et al. (2005) is presented in simplified form below. The terms decompose and synthesize respectively mean that one goes from a gridded field to a set of spherical harmonic coefficients and vice versa. The scheme is a way to solve the GSLE using the pseudo-spectral method. It follows an outer loop for the moving shorelines, a time step loop, and an inner loop to consistently apply the uniform and spatially differing mechanisms that are calculated individually, thus three loops in total.

1. Specify the the ice loading change δI and decompose to $[\delta I_j]$ at every time step. These remain constant through the iterations using the forcing input model.

2. Specify the present day topography and ocean function T_p and C_p, and set these to apply at all time steps for the first outer iteration.

3. **Beginning of outer loop and time step loop**

4. Decompose the ocean function C_j to $[\mathcal{C}_j]$

5. Calculate $TO_j = T_0(C_j - C_0)$ and decompose to $[\mathcal{TO}_j]$

6. Define the initial sea level change $[\delta S_j]$, being uniform when not yet defined,

$$[\delta S_j] = \frac{[\mathcal{C}_j]}{[\mathcal{C}_{00,j}]} \left(-\frac{\rho_i}{\rho_w} [\delta I] \right) \tag{A.11}$$

   and being equal to the last calculated δS at all other moments.

7. **Beginning inner loop**

8. Compute the full spatial effect of surface loadings and gravity perturbation. This is given by the spectral love number theory of Peltier (1974). They are numbers that describe the instantaneous (β) and delayed (E) response to loadings and mass redistributions, in the case of SELEN they are calculated in a subroutine called 'TABOO'.

$$[\mathcal{SL}_j] = \frac{3}{\rho_e} E \left(\rho_i [\Delta I_j] + \rho_w [\Delta S_j] \right) + \frac{3}{\rho_e} \sum_{n=1}^{j-1} \beta \left(\rho_i [\delta I_j] + \rho_w [\delta S_j] \right) \tag{A.12}$$

9. Calculate the effects on the sea bottom

$$RO_j = SL_j \cdot C \tag{A.13}$$

10. Calculate the fully uniform effect after surface loadings and gravity perturbations

were applied.

$$\left[\frac{\Delta\phi_j}{g}\right] = \frac{1}{[\mathcal{C}_{00,j}]}\left(-\frac{\rho_i}{\rho_w}[\delta I_{00,j}] - [RO_{00,j}] + [\mathcal{TO}_{oo,j}]\right) \tag{A.14}$$

11. Compute the new value for δS as

$$[\delta S_j] = -[\Delta S_j] + [RO_j] + \left[\frac{\Delta\phi_j}{g}\right][C_j] - [\mathcal{TO}_j] \tag{A.15}$$

12. **Iterate inner loop 3 times for convergence / end of loop**

13. Compute and synthesize $[\Delta SD_j]$

$$[\Delta SD_j] = [\Delta\mathcal{SL}_j] + \left[\frac{\Delta\phi_j}{g}\right] \tag{A.16}$$

14. Iterate over all time steps j / end of time loop

15. Compute the new topography T_j and corresponding ocean function C_j, using

$$T_j = T_p + \Delta SD_p - \Delta SD_j \tag{A.17}$$

16. **Iterate outer loop 3 times / end of program**

Appendix B

Batch operations

B.1 Reclassify grids

Shell script that converts the paleo DEM GeoTIFF files from Quantum GIS to SAGA GIS grid files, reclassifies them to 0 ($T_j < 0$) or 1 ($T_j \geq 0$), and converts them back to GeoTIFFs.

reclassify.sh

```
export SAGA_MLB=/usr/lib/saga

 for FILE in *.tiff
    do
        saga_cmd libio_gdal 0 -GRIDS=$FILE.sgrd -FILES=$FILE
        saga_cmd libgrid_tools "Reclassify Grid Values" -INPUT=$FILE.sgrd -RESULT=$FILE.
            reclass.sgrd -METHOD=2 -OLD=0.000000 -NEW=1.000000 -SOPERATOR=0 -MIN
            =0.000000 -MAX=10.000000 -RNEW=5.000000 -ROPERATOR=0 -RETAB=table.txt -
            TOPERATOR=2 -RETAB_2=NULL -F_MIN=0 -F_MAX=0 -F_CODE=0 -NODATA=0.000000 -
            OTHERS=0.000000
        saga_cmd libio_gdal 2 -GRIDS=$FILE.reclass.sgrd -FILE$FILE.reclass.tiff
    done
 mkdir ../class/
 mv *.reclass.tiff ../class
 rm *.mgrd *.prj *.sdat *.sgrd
```

B.2 Warp and polygonize

Shell script that turns the reclassified grids (output from SAGA GIS) from the regular WGS84 projection (EPSG:4326) to Lambert Azimuthal Equal-Area (EPSG:3575), and then polygonizes the output for all years.

vectorize.sh

```
 for FILE in *.tiff
    do
        gdalwarp -s_srs EPSG:4326 -t_srs EPSG:3575 -of GTiff -multi $FILE $FILE.reproj.
            tiff
        gdal_polygonize.py $FILE.reproj.tiff -f "ESRI Shapefile" $FILE.shp
    done
```

```
mkdir vect
mv *.tiff.* vect
```

B.3 Extract distance

PostGIS SQL script that queries the 'year' column of the island and continent shapefile and then calculates the shortest distance.

Extract_distance.sql

```
SELECT
      a.year
    , st_shortestline(a.geom,b.geom)
    , (st_distance(a.geom,b.geom)/1000) AS distance
FROM
    gavdos AS a
LEFT JOIN
    crete AS b
ON
    a.year = b.year
```

Appendix C

Extended results

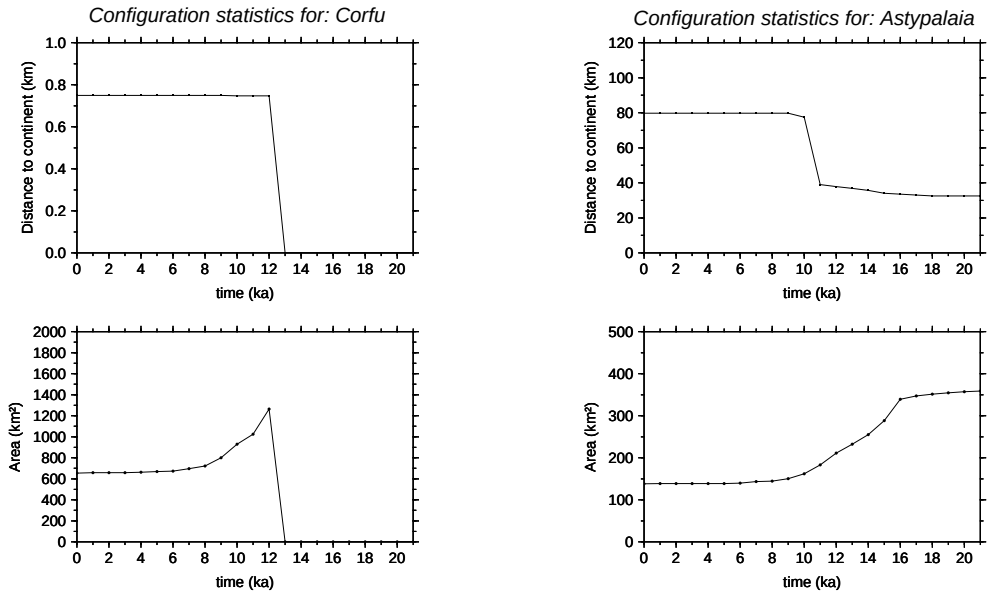

(a) 21 ka

(b) 16 ka

Figure C.1: The area and isolation as modeled with the GSLE, with values extracted using PostGIS for the distance and Quantum GIS for the area.

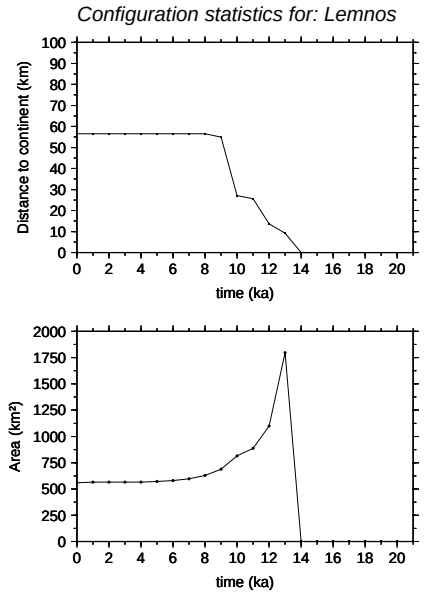

(a) 21 ka

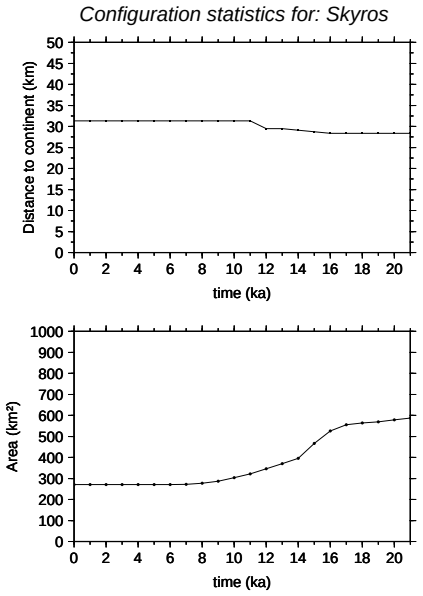

(b) 16 ka

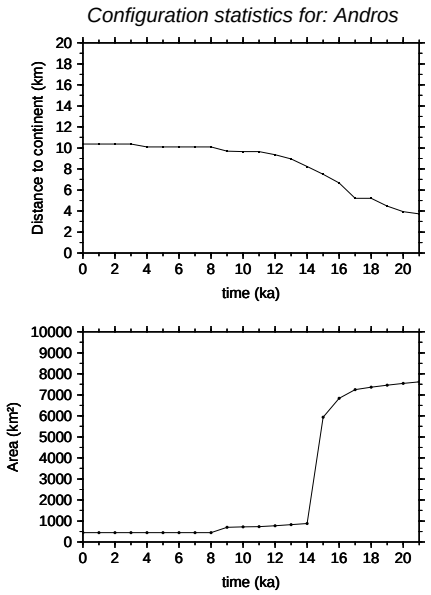

(c) 11 ka

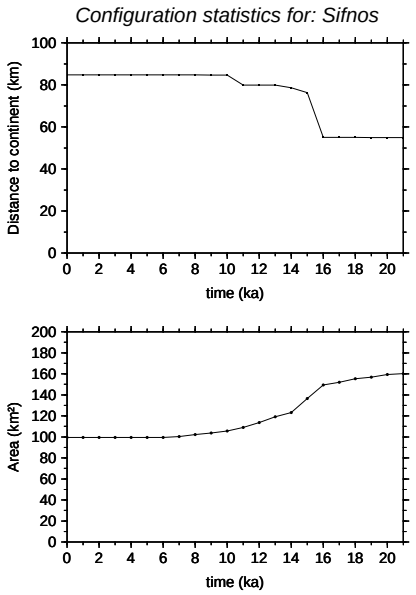

(d) 6 ka

Figure C.2: The area and isolation as modeled with the GSLE, with values extracted using PostGIS for the distance and Quantum GIS for the area.

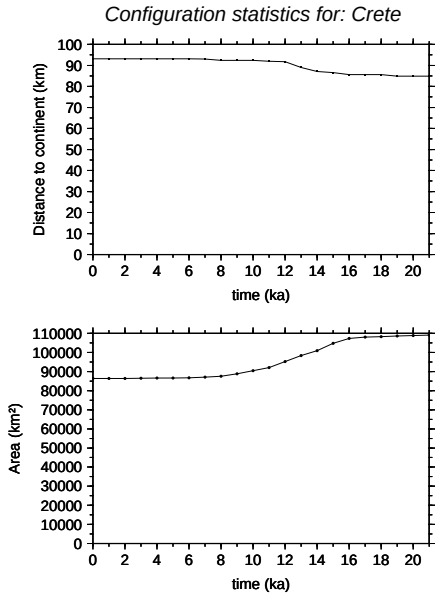

(a) 21 ka

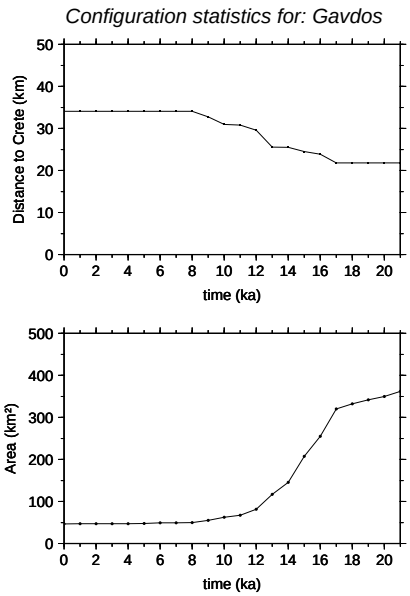

(b) 16 ka

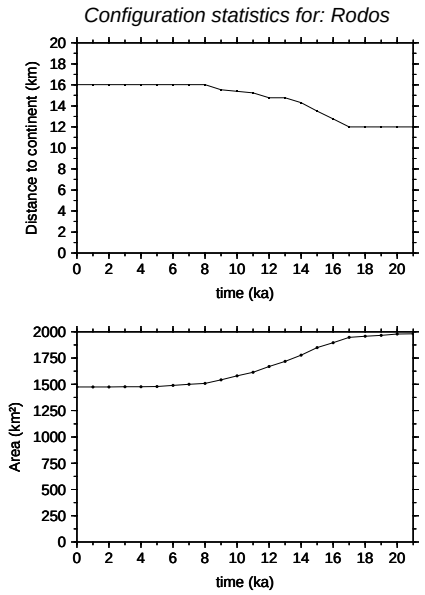

(c) 11 ka

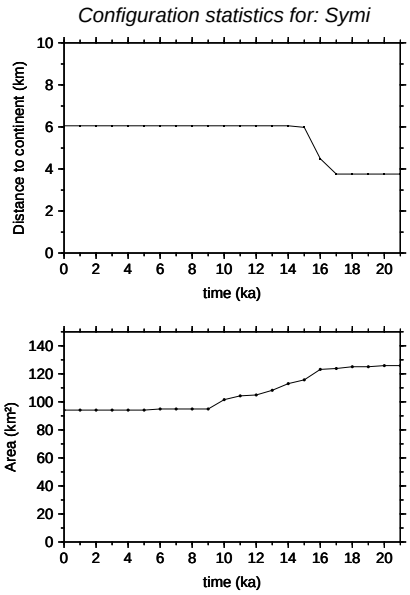

(d) 6 ka

Figure C.3: The area and isolation as modeled with the GSLE, with values extracted using PostGIS for the distance and Quantum GIS for the area.

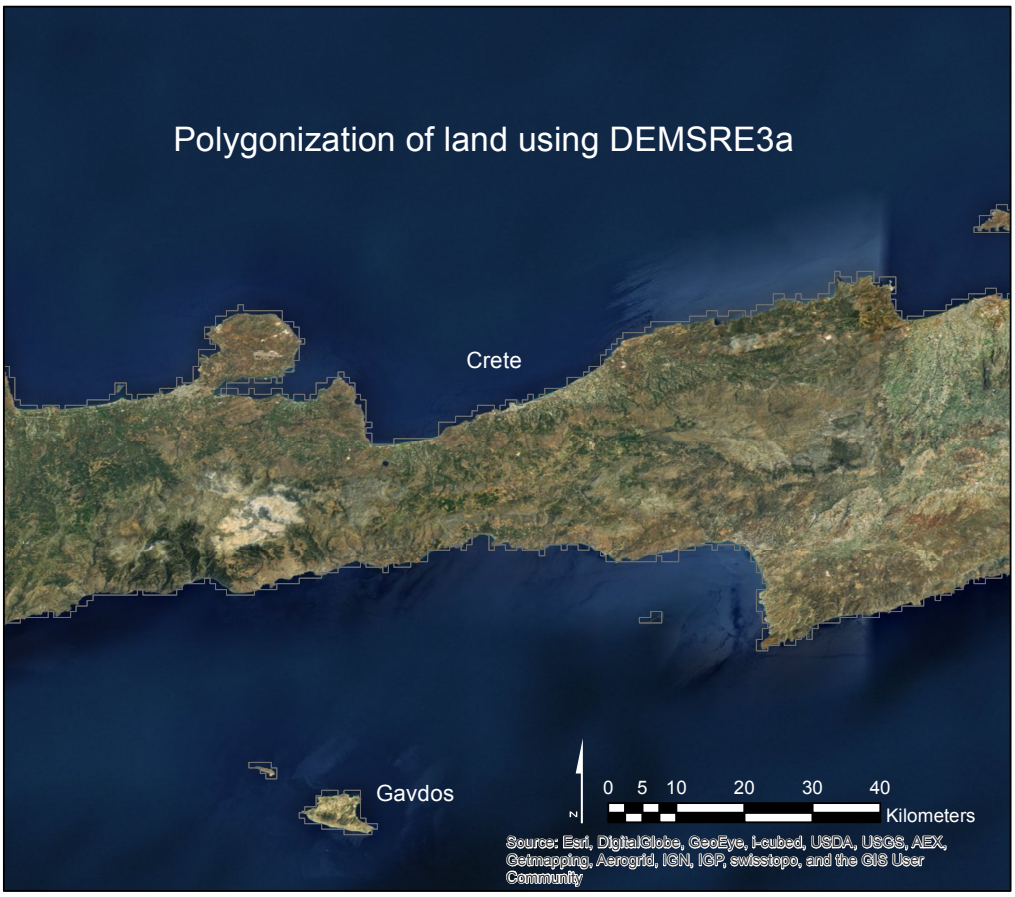

Figure C.4: Pixelation of islands in the Aegean area projected onto satellite photography from ESRI (2013)